Determining the Stereochemical Structures of Molecular Ions by "Coulomb-Explosion" Techniques with Fast (MeV) Molecular Ion Beams

DONALD S. GEMMELL

Physics Division, Argonne National Laboratory, Argonne, Illinois 60439

Received April 7, 1980

In most experimental techniques used to derive the stereochemical structures of molecular ions, the difficulty in obtaining a sufficient column density of the ions to be studied presents a severe limitation. Thus, for example, photon emission or absorption techniques usually involve searching for extremely weak and narrow lines in the presence of background radiation. Where such methods have been successfully applied, they result in very precise structure determinations. However, it has so far only proved possible to measure a handful of molecular ion structures with these "standard" techniques. This situation contrasts strongly with that for neutral molecules for which the experimental problems are much less severe and for which thousands of structures have been determined.

Recent studies on the dissociation of fast (MeV) molecular ion beams in thin foils suggest a novel alternative approach to the determination of molecular ion structures. At these high beam velocities (typically a few percent of the speed of light) each dissociating molecular ion projectile rapidly loses many (sometimes all) of its electrons in sudden violent collisions with electrons in the foil target. The projectile then undergoes a so-called "Coulomb explosion" as the now highly charged and monatomic fragments repel one another apart via their mutual Coulomb forces. These fragments emerge downstream from the foil with their velocities shifted in both magnitude and direction from the beam velocity. Typically the Coulomb explosion results in energy shifts of a few kiloelectronvolts and angular shifts of a few milliradians for the dissociation fragments. High-resolution measurements of the joint energy and angle distributions for these fragments (especially when two or more fragments are detected in coincidence) offer promising possibilities for deducing the stereochemical structures of the molecular ions constituting the incident beam.

If, instead of a foil target, a dilute gas target is used, the projectile dissociations then arise mainly from relatively gentle collisions. Nevertheless additional useful structure information can be obtained, especially when taken in conjunction with results from foil-induced dissociation.

In this article we review some recent high-resolution studies on the interactions of fast molecular ion beams with solid and gaseous targets and indicate how such studies may be applied to the problem of determining molecular ion structures.

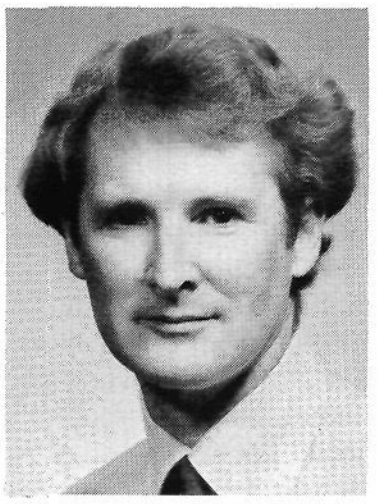

Donald S. Gemmell was born in Adelaide, South Australia. Following his undergraduate education at the University of Adelaide, he continued his studies at the Australian National University, Canberra, where he received his Ph.D. in 1959. After 3 years as a Research Fellow at AERE, Harwell, England, he joined the staff of the Physics Division, Argonne National Laboratory, where he is currently a Senior Physicist. His main research interests have included nuclear physics, the channeling of particles in crystals, and the interactions of fast molecular ions with matter.

Collision-Induced Dissociation at High Velocities

The collision-induced dissociation of molecular ions has previously been studied mostly with gaseous targets and with ion-beam energies in the kiloelectronvolt range (for a recent review, see ref 1). There are, however, definite advantages in extending such studies to the megaelectronvolt range. We summarize here the most significant of these advantages (for a more detailed discussion, see ref 2).

(1) The collision times become short compared with the times for molecular vibration and rotation and with the time for the subsequent dissociation [the cross sections for electron removal from the projectile are on the order of 10^{-16} cm^2 (see, for example, ref 3)].

(2) The use of thin foil targets becomes feasible. In foils, close collisions with target electrons cannot be avoided, and this leads to more energetic Coulomb explosions than those occurring with gas targets.

(3) For foil targets, higher beam energies lead to higher fragment charge states, giving more vigorous Coulomb explosions.

(4) As the projectile velocity v is raised, there is a decline not only in the absolute values of multiple scattering angles (which vary as v^{-2}) but also in the multiple scattering relative to the widths of the fragment angular distributions (which vary roughly as v^{-1}).

(5) Screening of the fragment charges by the target electrons in a foil is reduced at higher beam velocities.

For high projectile velocities ($v \gg v_0 = e^2/\hbar$), collision-induced dissociation may be well approximated as a two-step process. First there occurs a rapid collision with one or more target atoms during which the projectile's nuclei do not move in their center-of-mass (cm) frame. Because of their low mass, the electrons associated with the projectile reconfigure themselves in a time comparable with the collision time (this process includes the possibility of removal by ionization of some or all of the electrons). There then follows, on a much longer time scale, a dissociation of the resultant excited molecular state into two or more fragments.

Simple Coulomb Explosions

In this section we explore the implications of a simplified model for the Coulomb explosion of a fast molecular ion in a foil. We take as an example a tightly collimated beam of 3-MeV HeH^+ ions incident on a 100-Å carbon foil (Figure 1). The model can later be refined and extended to more complex projectiles.

Since the mean time to strip the two electrons from each projectile is short (a few times 10^{-17} s) compared with the dwell time in the foil (0.93 fs at the beam velocity $v = 1.07 \times 10^9$

0009-2665/80/0780-0301$05.00/0

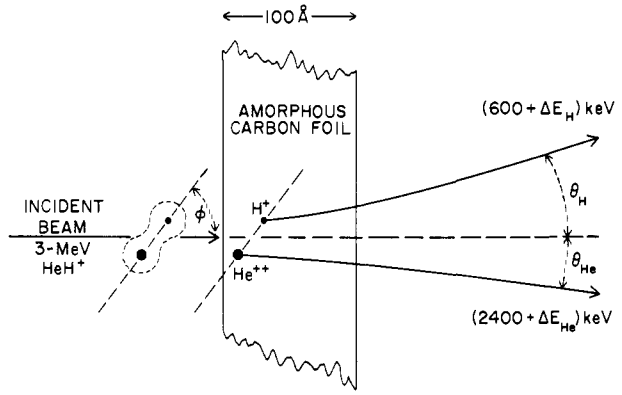

Figure 1. A (very) schematic picture of a 3-MeV HeH^+ projectile dissociating in a 100-Å-thick amorphous carbon foil.

cm/s) and with the times for molecular vibration ($\sim 10^{-14}$ s) and rotation ($\sim 10^{-12}$ s) of the projectile, we may make the approximation that the electron stripping and the start of the consequent Coulomb explosion both occur instantaneously at the front surface of the foil. Let the internuclear vector from the α particle to the proton in a given HeH^+ projectile have a length r_0 at this instant and be inclined at an angle ϕ relative to the beam direction. Let the values of r_0 have a probability distribution $D(r_0)$ which depends upon the population of the various vibronic states of the projectile.

If all the HeH^+ projectiles were in the ground electronic, vibrational, and rotational state, the most probable value of r_0 would be expected to be 0.79 Å (based, for example, on the potentials calculated by Kolos and Peek[4]). Let us consider a projectile having this particular value of r_0 at the moment of entry into the foil. Electron stripping then produces an α-particle-proton pair with a mutual Coulomb energy $\epsilon = 2e^2/r_0 = 36.5$ eV. This potential energy is converted into kinetic energy in the cm as the Coulomb explosion develops. Since this Coulomb energy is much larger than the energies that the fragments have due to vibration and rotation in the incoming projectile, we may make the further approximation that at the instant of stripping ($t = 0$) the α particle and the proton are at rest in the cm frame.

If, for the moment, we ignore further interactions of the projectile nuclei with the target foil, then the internuclear separation as a function of time, $r(t)$, is found by solving

$$\mu\ddot{r} = Z_1Z_2e^2/r^2 \tag{1}$$

with the initial conditions

$$r(0) = r_0,\ \dot{r}(0) = 0 \tag{2}$$

where $\mu = M_1M_2/(M_1 + M_2)$ is the reduced mass of the two fragments and Z_1e and Z_2e are their charges. From this one finds that the time for the internuclear separation to grow to r is given by

$$t(r/r_0) = t_0\, f(r/r_0) \tag{3}$$

where

$$t_0 = [\mu r_0^3/(2Z_1Z_2e^2)]^{1/2} \tag{4}$$

and

$$f(x) = \sqrt{x}\sqrt{x-1} + \ln(\sqrt{x} + \sqrt{x-1}) \tag{5}$$

If μ is expressed in amu and r_0 is in angstroms, then

$$t_0 = 1.90[\mu r_0^3/Z_1Z_2]^{1/2}\ \text{fs} \tag{6}$$

In a time t_0, 19% of the initial Coulomb potential energy is converted into kinetic energy of the separating fragments. The final asymptotic ($t \gg t_0$) relative velocity of recession is

$$\dot{r}(\infty) = [2Z_1Z_2e^2/\mu r_0]^{1/2} \tag{7}$$

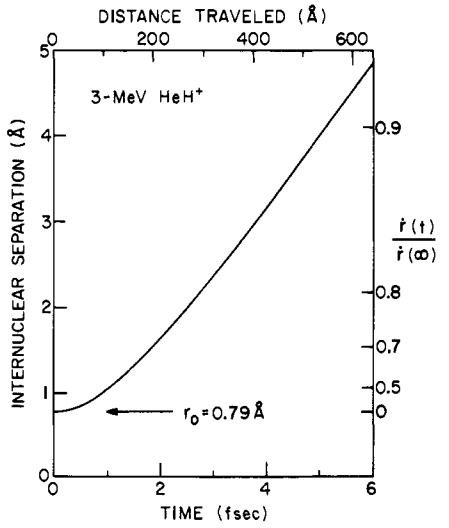

Figure 2. The dependence upon time of the internuclear separation between the α particle and the proton of a HeH^+ ion whose internuclear separation at $t = 0$ is 0.79 Å. The right-hand ordinate gives the fractional growth of the Coulomb-explosion velocity as a function of time. The scale at the top shows the distance traveled in the LAB frame by the projectile assuming the beam energy to be 3 MeV.

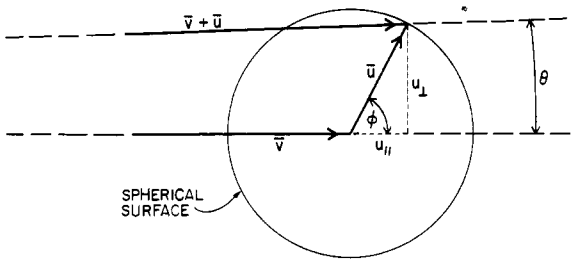

Figure 3. Vector diagram illustrating the relationship between cm and LAB coordinates for a fragment emerging from a Coulomb-exploded molecular ion projectile.

For our example of 3-MeV HeH^+ ($Z_1 = 1$, $Z_2 = 2$), $t_0 = 0.84$ fs and $\dot{r}(\infty) = 9.4 \times 10^6$ cm/s (about 1% of the beam velocity). The internuclear separation as a function of time is shown for this example in Figure 2. From Figure 2 one also sees that with our dwell time in the target of 0.93 fs, a significant portion of the Coulomb explosion occurs after the fragments emerge from the foil (the internuclear separation at exit is 1.01 Å).

In this simple picture, the spatial orientation of the internuclear vector for the diatomic projectile remains constant throughout the stripping and the ensuing Coulomb explosion. (The corresponding statement for polyatomic projectiles is not necessarily true.)

The final energies and angles of the fragments in the laboratory (LAB) frame are easily obtained by referring to the vector diagram in Figure 3. Let $\bar{u}$ be the asymptotic cm velocity acquired by the fragment of mass M_1 as a result of the Coulomb explosion. That is

$$u = (\mu/M_1)\dot{r}(\infty) \tag{8}$$

The asymptotic LAB velocity of this fragment is then $\bar{v} + \bar{u}$. The shift in LAB angle is

$$\theta \approx (u \sin\phi)/v = u_\perp/v \tag{9}$$

and the shift in LAB energy is

$$\begin{aligned}\Delta E &= \tfrac{1}{2}M_1(\bar{v} + \bar{u})^2 - \tfrac{1}{2}M_1v^2 \\ &\approx M_1vu\cos\phi = M_1vu_\parallel = 2E_1(u_\parallel/v)\end{aligned} \tag{10}$$

where

$$E_1 = \tfrac{1}{2}M_1v^2 \tag{11}$$

(we neglect terms with relative magnitudes on the order of u/v).

From this one sees that for each fragment species there is a maximum LAB angle θ_{max} such that for $\theta > \theta_{max}$ none of these fragments will be observed. For $\theta < \theta_{max}$ two classes of this fragment species will be observed: one with an upward shift in energy and one with an equal shift downward in energy. For $\theta = \theta_{max}$ these two classes coalesce into a single group having no energy shift. If $\theta = \theta_{max}$, then $\phi \approx 90°$; i.e., at $t \approx 0$, the internuclear vector of the incident projectile lies normal to the beam direction. For the fragment of mass M_1

$$\theta_{max} = u/v = (\epsilon_1/E_1)^{1/2} \tag{12}$$

where

$$\epsilon_1 = (\mu/M_1)(Z_1Z_2e^2/r_0) \tag{13}$$

In the LAB frame the fragments emerging along the beam direction ($\theta = 0$) correspond to the other extreme orientation of the incoming projectile ($\theta = 0$ or $\theta = 180°$). Such fragments, although suffering no angular shift in the LAB, are observed with the maximal energy shift $\pm\Delta E_{max}$. The sign of the shift depends on whether the fragments are leading (+) or trailing (–) their partners. For the fragment of mass M_1

$$\Delta E_{max} = M_1vu = 2(\epsilon_1E_1)^{1/2} \tag{14}$$

In our example of 3-MeV HeH^+ with $r_0 = 0.79$ Å, eq 12 and 14 give for the protons $\theta_{max} = 7.0$ mrad (0.40°) and $\Delta E_{max} = 8.4$ keV. For the α particles, θ_{max} is a factor of four smaller and ΔE_{max} is the same.

It is interesting to note the "amplifying" effect of the cross-term in eq 10 and 14. A cm energy on the order of electronvolts gives rise to a LAB energy shift on the order of kiloelectronvolts when MeV projectiles are employed.

If the spatial orientations of the incident projectiles are isotropically distributed, we may think of the tip of the vector $\bar{u}$ in Figure 3 as populating with uniform probability the surface of a spherical shell of radius u. Thus, for a given projectile orientation, there is a $(4\pi u^2)^{-1}$ weighting factor for the values of u that arise from an initial distribution $D(r_0)$ of internuclear spacings. The distribution function for u is

$$G(u) = (4\pi u^2)^{-1}D(r_0)|dr_0/du| \tag{15}$$

where $G(u)$ and $D(r_0)$ are normalized by

$$\int_0^\infty D(r_0)dr_0 = 1, \qquad 4\pi\int_0^\infty G(u)u^2\,du = 1 \tag{16}$$

For a simple Coulomb explosion we use eq 7 and 8 to obtain

$$G(u) \propto u^{-5}D(r_0(u)) \tag{17}$$

From the foregoing it is apparent that measurement of the LAB variables θ and ΔE for one of the fragment species (M_1, say) is equivalent to a measurement of $u_\perp$ and $u_\parallel$ in the cm system. Knowledge of the Coulomb dissociation potential then permits determination of $D(r_0)$. Actually just one of the two measurements suffices: either the distribution of θ for $\Delta E = 0$, or the distribution of ΔE for $\theta = 0$.

A two-parameter measurement (θ, ΔE) of the yield of fragments of mass M_1 is expected to give a uniform "ring pattern" since it corresponds to a cut across the center of the sphere indicated in Figure 3. In Figure 4 we show such a ring pattern calculated for the protons from our 3-MeV HeH^+ example. For the calculation we have assumed that all projectiles are in the ground vibronic state and we have used $D(r_0)$ obtained from the potential given by Kolos and Peek.[4] Energy and angle distributions such as those in Figure 4b,c are sometimes called a "cross" since they represent orthogonal diametric cuts across the ring pattern.

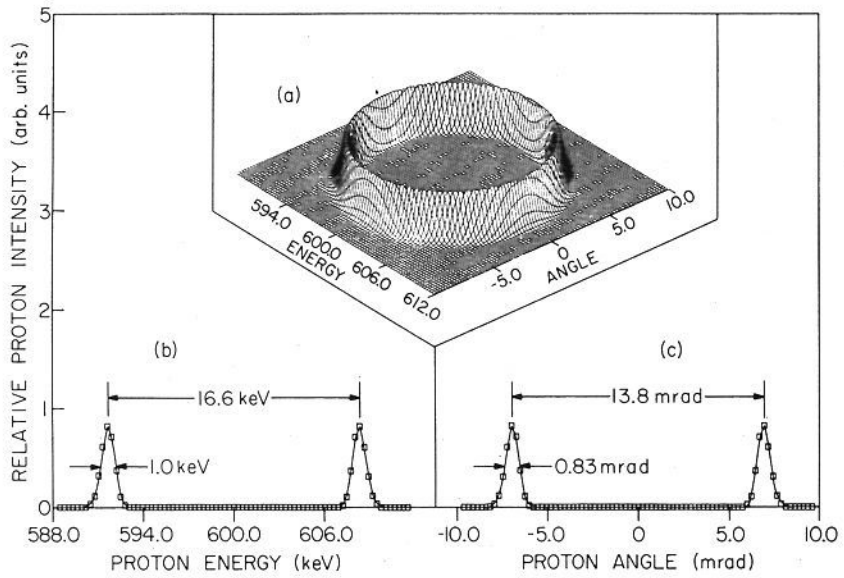

Figure 4. (a) "Ring pattern" calculated for the joint energy–angle distribution for protons arising from the simple Coulomb explosion of 3-MeV HeH^+. (b) Energy distribution for $\theta = 0$. (c) Angular distribution for $\Delta E = 0$.

Influence of the Solid Medium

We have thus far ignored the influence of the medium apart from its role in initiating the Coulomb explosion. In practice various phenomena occurring as fast ions traverse foil targets can influence the dissociating fragments. The most important effects are multiple scattering, energy loss and energy straggling, wake effects, electronic screening, and charge exchange. (If the foil were crystalline, a case we do not consider here, ion channeling effects would play a prominent role[5,6].)

Multiple scattering can be a serious problem in that it effectively blurs the experimental angular resolution. It is minimized by using the thinnest possible target foils with low atomic number and by using high projectile velocities. Thus, most of the work discussed here has employed carbon targets about 100 Å thick. For such targets, 600-keV protons (e.g., from 3-MeV HeH^+) suffer multiple scattering with an average angular deflection of about 0.6 mrad.

Energy loss and straggling due to the normal stopping power of the medium are much less severe problems. For 600-keV protons traversing 100-Å carbon, the energy loss is 0.7 keV and the straggling is only a few tens of eV.

Polarization wake effects and electronic screening have been discovered[6] to have a significant influence on the motion of a cluster of fragments. The concept of a polarization wake trailing behind a fast ion traversing a solid was discussed in 1948 by Niels Bohr[3] and has since been treated by several authors (e.g., ref 7–16). The wake represents the response of the target electrons to the passage of the charged projectile. In a simple treatment the target can be considered as an electron gas in which the projectile induces plasma oscillations that trail behind it. Figure 5 shows an example of the wake potential calculated with such a model.[9] This potential (somewhat analogous to the wake of a boat moving in water) moves along with the projectile. The derivative of the potential evaluated at the projectile gives the stopping power. The wakes of a Coulomb-exploding cluster of ions traversing a foil superpose upon one another. Thus, for a diatomic projectile, the motion of one of the fragments while inside the foil is affected by the wake of its partner. This results in a tendency for trailing fragments to align more closely behind their partners.[6]

For more slowly moving fragments, screening by target electrons begins to play a significant role. The Coulomb explosion develops between charges for which the potential is exponentially screened, the screening distance being given by

$$a = v/\omega_p \tag{18}$$

where ω_p is the plasma frequency appropriate to the target electrons. For 1-MeV carbon ions, for example, traversing a

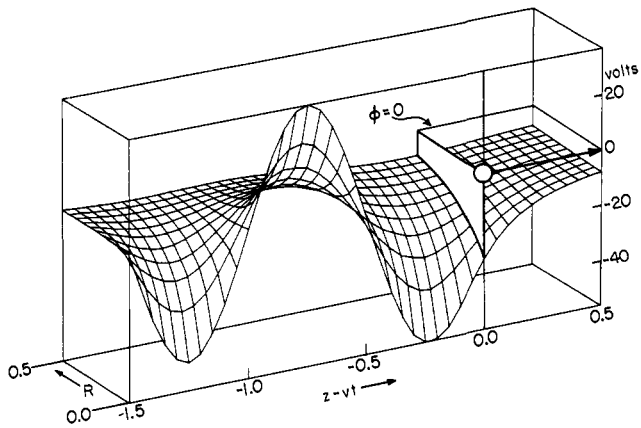

Figure 5. Potential distribution associated with the polarization wake of a 400-keV proton traversing carbon.[9] Distances are shown in units of $\lambda = 2\pi v/\omega_p = 14.5$ Å (for carbon, $\hbar\omega_p = 25$ eV).

carbon foil ($\hbar\omega_p = 25.9$ eV), we find $a = 1.0$ Å.

Charge exchange (electron capture and loss) in the target can have a major effect upon the ionic fragments traversing a foil. This is particularly true of heavy fragments. Inside the foil the extremely rapid ($\sim 10^{-17}$ s) capture and loss of electrons by the fragments leads to a well-defined effective charge that determines the stopping power and also the magnitude of the Coulomb explosion. At high velocities the effective charge for a given ion can be written as

$$Z^{eff} = (S/S_p)^{1/2} \tag{19}$$

where S is the stopping power of the foil for the ion and S_p is the corresponding value for a proton of the same velocity.[17] Outside the foil the ions adopt integral charge states.

Apparatus for High-Resolution Measurements

To explore the details of ring patterns having "radii" of a few milliradians and a few kiloelectronvolts, experimental resolution widths at least an order of magnitude smaller than these values are desirable. This poses some technical problems, particularly in the angular coordinate. The solutions to these problems as implemented at Argonne[18] have been described in the literature (e.g., ref 2, 12, 19–23). Figures 6 and 7 show the experimental arrangement now in use.

Magnetically analyzed molecular ion beams are collimated to have a maximum angular divergence of ±0.09 mrad and a spot size of 1 mm at the target position. A set of "pre-deflector" plates permits electrostatic deflection of the beam incident on the target. Similarly a set of "post-deflectors" is used to deflect charged particles emerging from the target. The pre- and post-deflectors are used in combination so as to avoid detecting particles that arise from spurious incident beams (e.g., fragments arising from dissociation of the primary beam along the long flight path between the beam collimators). A 25° electrostatic analyzer having a relative energy resolution of $\pm 3 \times 10^{-4}$ is located several meters downstream from the target. An aperture placed ahead of the analyzer accepts a 1-mm-diameter group of trajectories originating at the target position.

Distributions in energy and angle are made for particles emerging from the target by varying the voltages on the horizontal pre-deflectors and/or the post-deflectors in conjunction with that on the electrostatic analyzer. [The vertical ("Y") deflectors are normally used only for "trimming" purposes.] The overall angular resolution is ±0.15 mrad.

The detector chamber shown in Figure 7 is a recent addition to the beam line. It permits the coincident detection of dissociation fragments. The chamber houses two detectors that can be positioned to an accuracy of about 0.001 in. anywhere on a 20-in. diameter circular area subtending an angle of 100 mrad at the target.

With our apparatus resolutions

$$\delta\theta = \pm 1.5 \times 10^{-4} \text{ rad}, \qquad \delta E/E_1 = \pm 3 \times 10^{-4} \tag{20}$$

we are able to measure $u_\perp$ and $u_\parallel$ with equal accuracy. From eq 9 and 10 we find

$$\delta u_\perp = \delta u_\parallel = (\pm 1.5 \times 10^{-4})v \tag{21}$$

Measurements on "Ring Patterns" for Diatomic Projectiles

Figure 8 shows a ring pattern and a cross measured for protons from 3-MeV HeH^+ incident upon a 195-Å thick carbon foil.[2] The ring has approximately the diameter predicted from our simple model (cf. Figure 4). The most obvious feature not predicted from the model is the nonuniform distribution of proton intensity around the ring. There is an enhanced intensity for trailing protons and (to a much lesser degree) for leading protons. This redistribution of particle flux is a consequence of the interaction of the fragments with the wakes that their partners induce in the foil. It is to be observed for both heteronuclear and homonuclear projectiles.

The widths of the peaks in the measured cross are larger than expected for the HeH^+ ground state alone (Figure 4). This is because $D(r_0)$ is a broader distribution (excited states of the projectile contribute) and because of multiple scattering. The asymmetry in the peak widths in the $\theta = 0$ energy spectrum is caused by wake effects.

Wake effects are also responsible for the slightly asymmetric location of the peaks in the energy spectrum with respect to the expected center of the ring. At this central position one observes a very small peak (Figure 8). It arises from dissociations in the target which produce He^0 and a proton.[2,19,22] Considering the weighting factors given in eq 15, it is evident that the fraction of dissociations resulting in He^0–H^+ pairs is very small. These weighting factors coupled with the breadth of $D(r_0)$ cause a slight reduction in the ring diameter as compared with the values given in Figure 4 and by eq 12 and 14.

Figures 9–11 show similar results for the foil-induced dissociation of beams of H_2^+, $^3He_2^+$, and N_2^+. For further examples

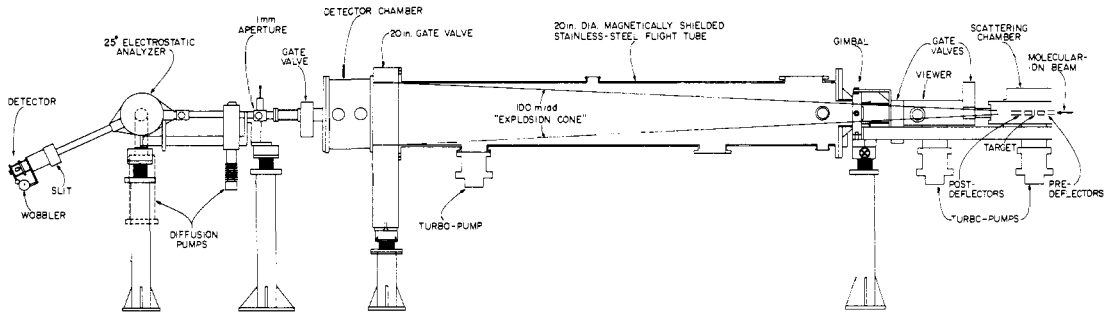

Figure 6. Schematic diagram of the experimental arrangement at Argonne's 4-MV Dynamitron accelerator.

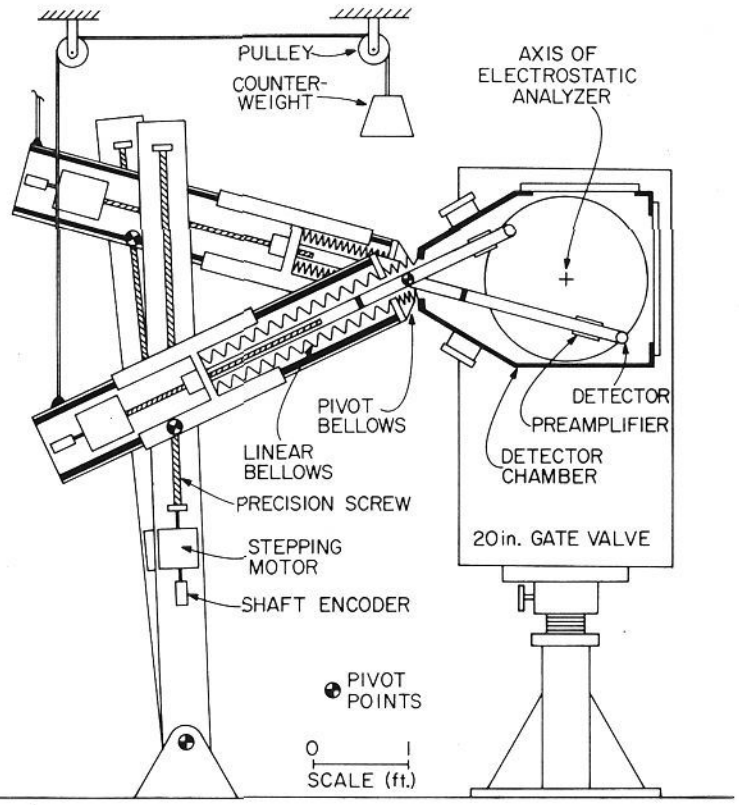

Figure 7. Schematic diagram showing a cross-sectional view of the detector chamber and movable detector systems at Argonne's 4-MV Dynamitron accelerator.

of data of this type, see ref 2, 12, 13, 15, 16, and 19–27.

Figure 12 shows a comparison between the measured and calculated[9] ring patterns for a typical case of foil-induced dissociation. When the data were fitted, the only adjustable parameters were the most probable value of r_0 and the standard deviation σ of the distribution $D(r_0)$, assumed here to be Gaussian. The best fit (Figure 12b) is obtained with $\bar{r}_0 = 0.79$ Å and $\sigma = 0.15$ Å. For the vibrationless ground state of HeH^+, a Gaussian approximation to $D(r_0)$ would require $\bar{r}_0 = 0.79$ Å and $\sigma = 0.081$ Å. The increased width of the experimentally derived σ implies the population of excited states in the incident projectiles. A detailed analysis[2] of data such as those in Figures 8 and 12 shows that the four lowest lying vibrational states in the HeH^+ ions represent 53%, 22%, 11%, and 6%, respectively, of the incident beam. The most probable value of r_0 remains 0.79 Å. (The data shown for HeH^+ in Figures 8 and 12 were obtained by using a duoplasmatron ion source fed with a gas mixture of 90% He and 10% H_2. Recently it was discovered[28] that an RF source fed with the same gas mixture produces HeH^+ ions in much higher states of vibrational excitation.) A similar analysis has been performed for H_2^+ beams where it is found that the vibrational population is fairly close to that expected on the basis of Franck–Condon factors.[2]

For slowly moving heavy-ion fragments, an improved fit to the data can be obtained by using a wake model that takes better into account the close collisions with target electrons. Thus, for example, Breskin et al.[15,16] have accounted in a very precise way for the foil-induced dissociation of 11.2-MeV OH^+.

When fast molecular ions dissociate in a dilute gas target, wake effects, screening, and multiple scattering no longer play a role. Figure 13 shows two examples. One sees immediately that the rings are uniformly populated. The diameters of the rings correspond to the dissociations $H_2^+ \rightarrow H^+ + H^+$ and $HeH^+ \rightarrow He^+ + H^+$ (there is a very much weaker outer ring in Figure 13b corresponding to $HeH^+ \rightarrow He^{2+} + H^+$). The patterns display dominant central peaks. The central regions can be quantitatively accounted for[2] in terms of collision-induced transitions of the projectiles to excited electronic states which then decay dissociatively, yielding one neutral and one charged fragment. Gentle collisions of this type are possible in gases (unlike solids) where large-impact-parameter collisions are favored. For such excitations the resultant cm energy acquired by the fragments can be small (<0.1 eV, say) if the initial internuclear separation is large [i.e., on the tail of the distribution $D(r_0)$]. These fragments, although arising in only a small fraction of the dissociations, are detected for all initial projectile orientations and thus give rise to the large central peak.

Implications for Structure Determinations

Analysis of many ring patterns and crosses has shown (see, for example, ref 20) that for a great variety of diatomic molecular ion projectiles the bond length can be determined with an accuracy of about 0.01 Å. In the analysis the influences (usually relatively small) of wake effects, multiple scattering, post-foil charge-state distributions, etc., are taken into account.

At Argonne we have become interested in exploring the extent to which these high-resolution studies with fragmentation techniques may be extended to the difficult problem of determining the geometric structures of polyatomic molecular ions.[12,22,23] Related studies are also under way at Brookhaven[29] and at the Weizmann Institute.[16,30] Although the accuracy expected from the fragmentation techniques may be poor (e.g., ~0.01 Å in bond lengths and ~1° in bond angles for not-too-complicated species) compared with that attainable with

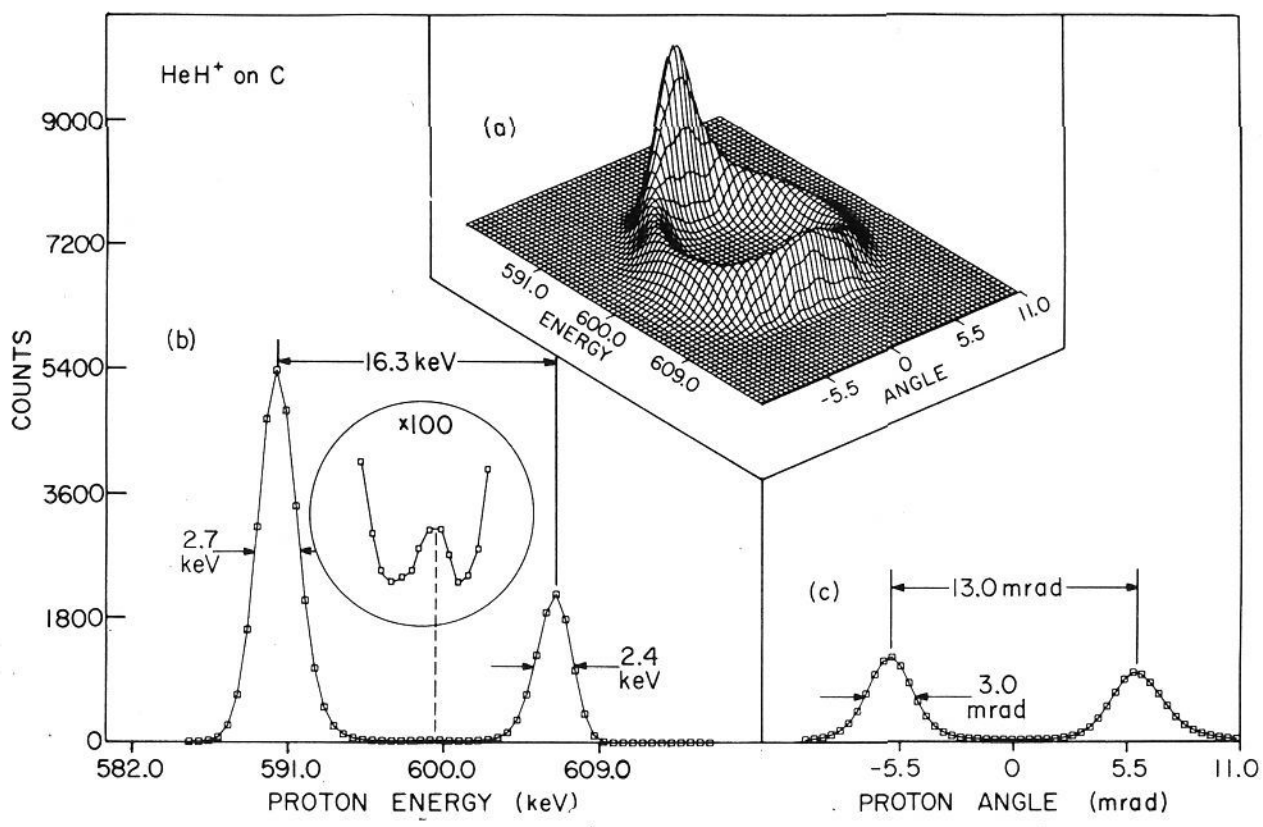

Figure 8. (a) "Ring pattern" and (b, c) "cross" for protons from 3.0-MeV HeH^+ dissociating in a 195-Å-thick carbon foil.[2]

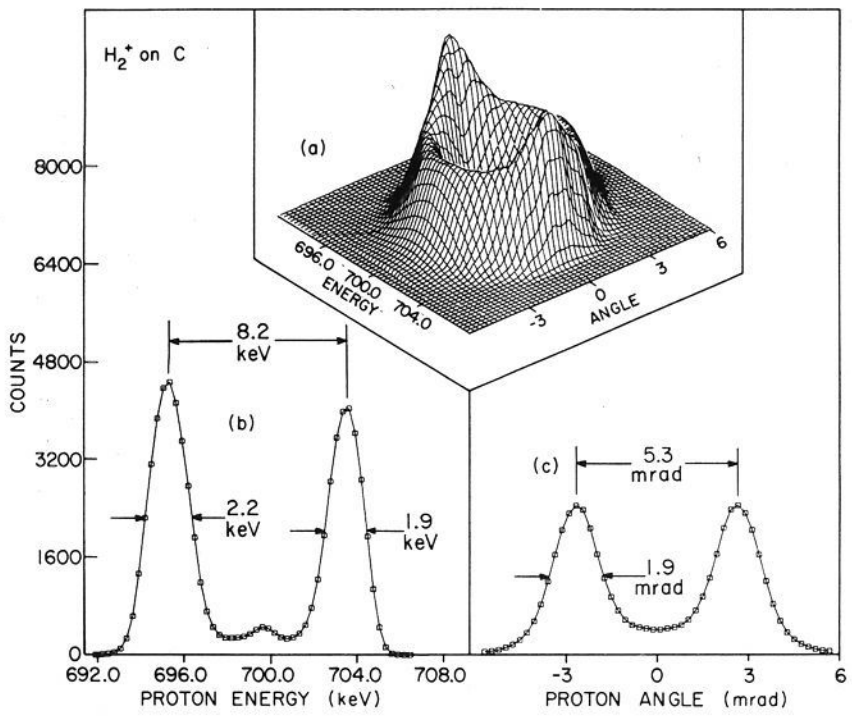

Figure 9. (a) "Ring pattern" and (b, c) "cross" for protons from 1.4-MeV H_2^+ dissociating in an 88-Å-thick carbon foil.[2]

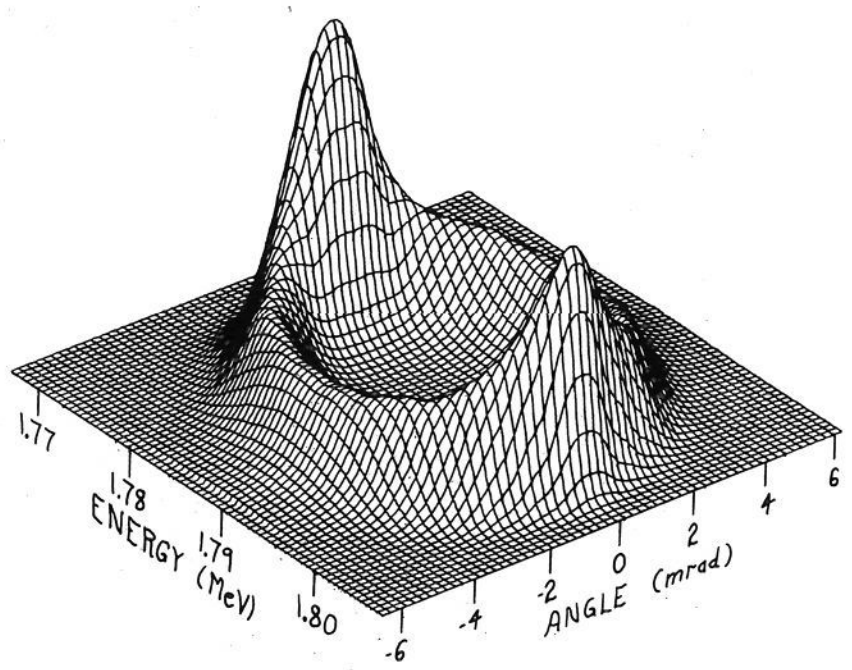

Figure 10. "Ring pattern" for $^3He^{2+}$ from 3.6-MeV $^3He_2^+$ dissociating in a 118-Å-thick carbon foil.[21]

"standard" photon techniques (when they can be applied), it should be good enough to resolve many conflicts between predictions from various structure calculations. Further, this level of accuracy should suffice to assist practitioners of the photon techniques to zero in on the frequencies of their (usually very narrow) resonances. One further point: the molecular ions that are of the greatest interest in astrochemical and fusion studies are very much the same ones produced copiously from the plasma ion sources normally used in electrostatic accelerators. Figure 14 illustrates this.

Except for the very simplest polyatomic molecular ions (e.g., H_3^+), high-resolution studies on single fragments yield only gross features of the stereochemical structures. For example, our measurements on C^{2+} fragments from 3.6-MeV $C_3H_3^+$ ions dissociating in thin foils demonstrate only that the carbons sit on the corners of an approximately equilateral triangle [that is, we have a beam of cyclopropenyl ions and not propargyl ions (which are linear in carbons)]. Similarly, our measurements on single fragments from OH_2^+ show only that the protons are equivalent and that the oxygen is "in the middle". The accuracy in determining bond lengths and bond angles is poor because there are wide ranges of values for these parameters that combine to give about the same Coulomb explosion velocity u for any given fragment.

A further difficulty associated with this type of measurement for polyatomic molecular ions lies in analyzing the effects of vibrational excitations of the projectiles. Excitations of some modes (e.g., symmetric breathing modes) can frequently be expected to result only in apparent changes in the bond lengths determined by the Coulomb-explosion method. However, many nonsymmetric modes can result in apparent structures that differ markedly from the structure of the vibrationless ground state. It is therefore important to analyze the Coulomb-explosion data in terms of the specific modes that can be excited for each projectile species considered. The analysis can be greatly simplified if the projectiles can be prepared in their ground (or at most a small range of low-lying) vibrational states—often a difficult technical task.

Polyatomic structures can be much more precisely determined if spatial and temporal coincidences are recorded for two or more dissociation fragments from a given projectile. With this in mind, we recently revised the apparatus at Argonne so as to permit a wide variety of coincidence measurements (Figure 7). We are now able to measure double or triple coincidences and record simultaneously information on fragment charge states, energies, and flight times from the target. The system has been tested with various simple diatomic and triatomic projectiles (H_2^+, HeH^+, CH^+, NH^+, OH^+ H_3^+, CH_2^+, NH_2^+, OH_2^+, etc.).

In the remaining sections we present some measurements on single fragments and then some preliminary results on coincidence measurements.

Measurements on Single Fragments from Polyatomic Projectiles

H_3^+. A joint study[31] of the simplest polyatomic molecular ion, H_3^+, was undertaken at the University of Lyon, the Weizmann

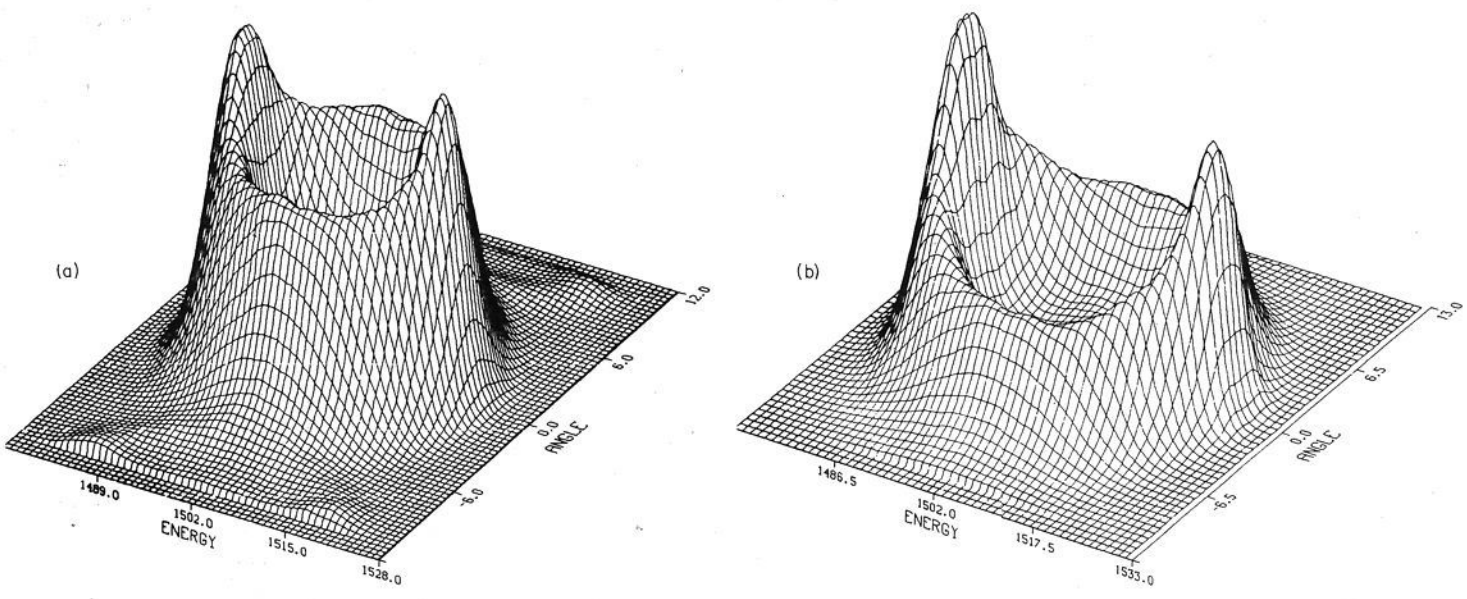

Figure 11. "Ring patterns" for (a) N^+ and (b) N^{4+} fragments arising from the dissociation of 3-MeV N_2^+ in a 75-Å-thick carbon foil.[24]

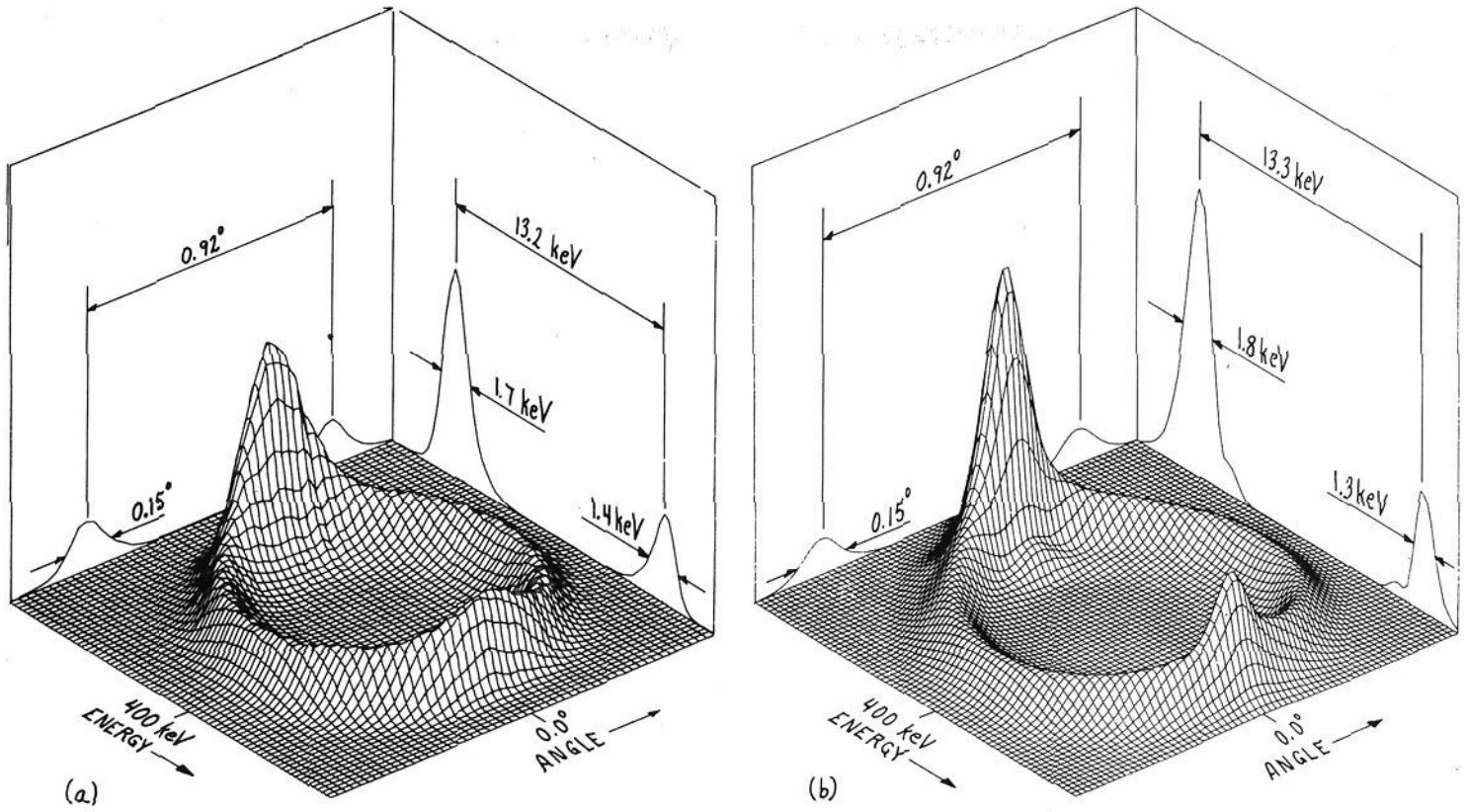

Figure 12. (a) Experimental and (b) calculated (based on a Coulomb explosion modified by wake effects and multiple scattering) ring patterns for protons from 2.0-MeV HeH^+ dissociating in an 85-Å-thick carbon foil.[9]

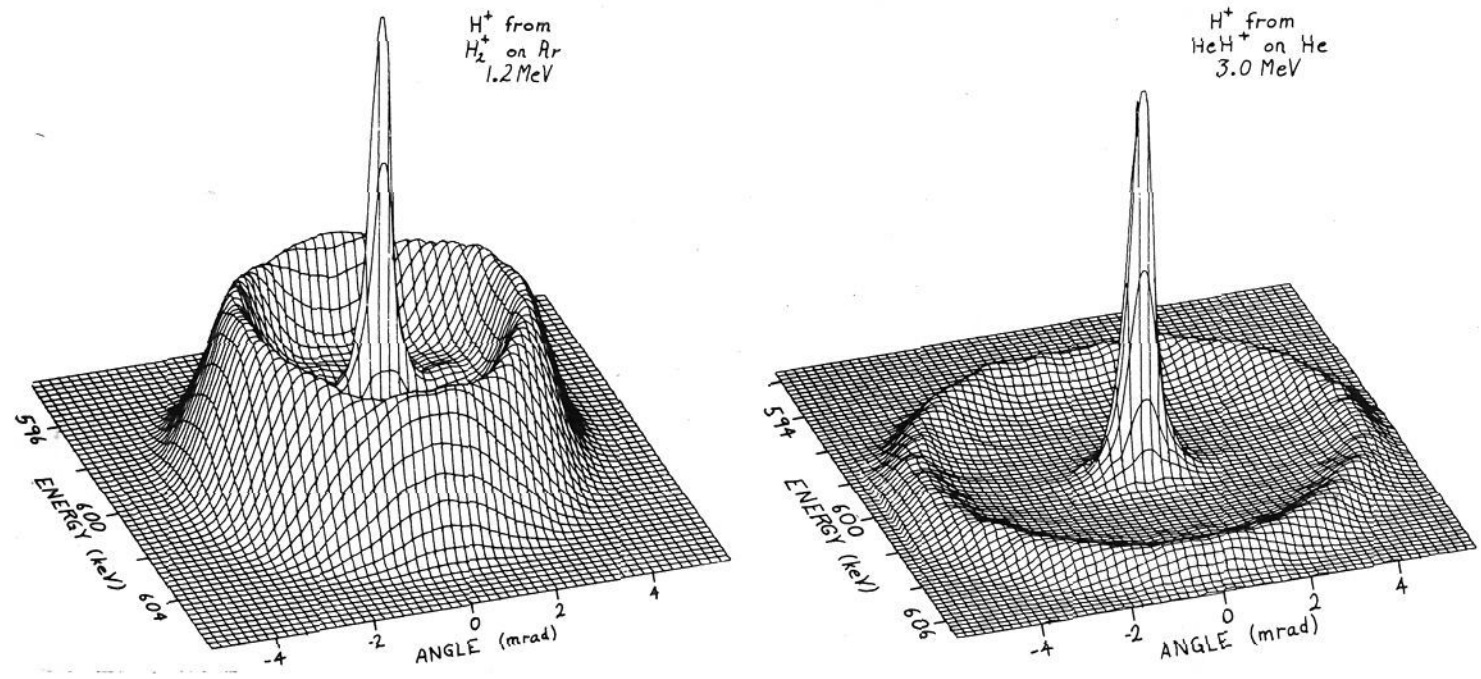

Figure 13. Joint energy–angle distributions for protons from 1.2-MeV H_2^+ and 3.0-MeV HeH^+ dissociating in gaseous Ar and He, respectively.[2]

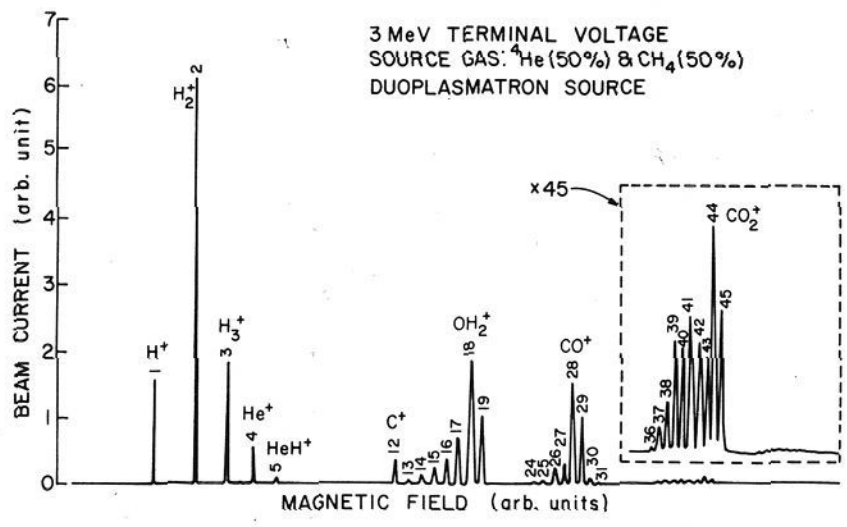

Figure 14. A "mass-scan" of the ion beams emerging from Argonne's 4-MV Dynamitron accelerator operating with a duoplasmatron ion source fed with a mixture of He and CH_4 gases.

Institute, and Argonne National Laboratory. Each laboratory performed a measurement based on the Coulomb explosion of fast H_3^+ ions. Although somewhat different techniques were used, the three measurements gave results in agreement with one another. It was experimentally demonstrated (for the first time) that H_3^+ is equilateral triangular in shape. The three measurements of the proton–proton bond distance yielded 0.97

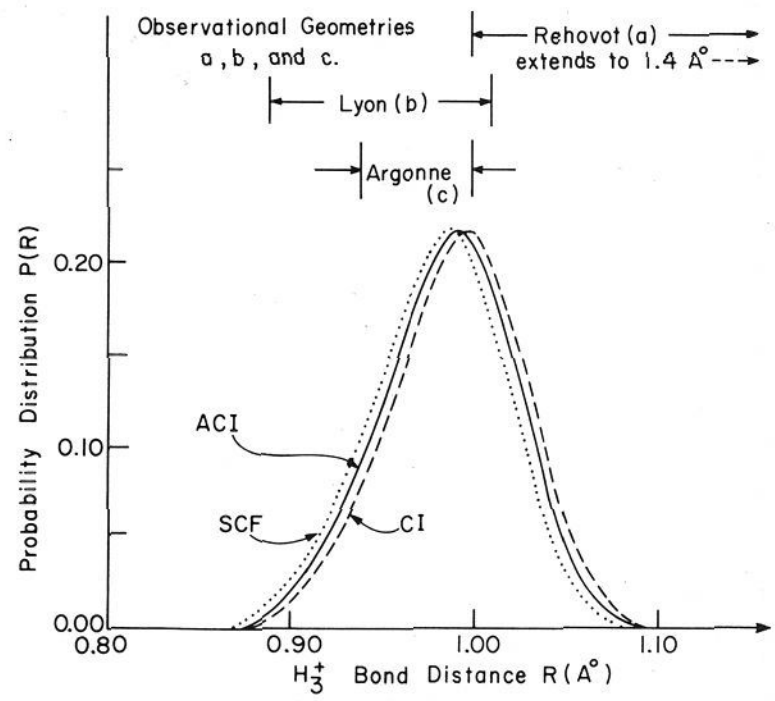

Figure 15. Comparison between measured[31] and calculated[32] distributions in the proton–proton bond distance in H_3^+ (from ref 32).

± 0.03 Å (Argonne), 0.95 ± 0.06 Å (Lyon), and 1.1 ± 0.2 Å (Weizmann Institute). Figure 15 shows a comparison of these results with a recent calculation by Carney[32] based on the

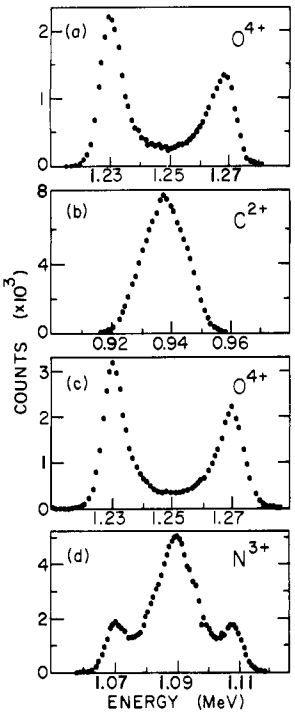

Figure 16. Energy spectra at $\theta = 0$ for (a) O^{4+} and (b) C^{2+} resulting from 3.5-MeV CO_2^+ bombarding a 133-Å-thick C foil, and for (c) O^{4+} and (d) N^{3+} resulting from 3.5-MeV N_2O^+ bombarding a 160-Å-thick carbon foil.[35] The spectra are not normalized to one another.

vibrational-state population parameters of Smith and Futrell.[33] (The vibrational ground state of H_3^+ has a calculated[34] bond length of 0.91 Å.)

CO_2^+ and N_2O^+. A typical example of the manner in which gross structures may be rapidly determined by Coulomb-explosion techniques is to be found in recent studies at Argonne[35] with 3.5-MeV beams of CO_2^+ and N_2O^+. These molecular ions in their ground and low-lying states are known[36] to be linear; but while CO_2^+ has the symmetric form (O–C–O), N_2O^+ is asymmetric (N–N–O). Figure 16 shows $\theta = 0$ energy spectra for O^{4+} and C^{2+} and CO_2^+ and O^{4+} and N^{3+} from N_2O^+. Similar spectra were obtained for fragments emerging in other charge states. Each spectrum takes about 5 min to accumulate. The principal structural characteristics are evident from just a casual inspection of Figure 16. The existence of only two peaks in Figure 16a indicates that the two oxygen atoms in CO_2^+ are equivalent. The existence of just one peak in Figure 16b shows that the carbon atom is central in a linear molecule (no net Coulomb-explosion velocity). The two peaks in Figure 16c show that the oxygen atom in N_2O^+ lies "on the outside" and the three peaks in Figure 16d show that one nitrogen atom is "on the outside" and that one is in the center of a linear molecule. The central peak in Figure 16d is much more strongly populated than the two side peaks because many more incident orientations contribute to it.

From these considerations, it can be seen that by simply counting the number of peaks in each spectrum, one can infer that both CO_2^+ and N_2O^+ are linear with structures O–C–O and N–N–O. A more detailed analysis is obviously required to obtain precise values for the bond lengths and angles.

CH_n^+ (n = 0, 4). The proton and the carbon fragments arising from the Coulomb explosion of CH^+, CH_2^+, CH_3^+, and CH_4^+ have been studied at beam velocities corresponding to 0.194 MeV/amu.[37] The singlet proton spectra, although reflecting vigorous Coulomb explosions, are not particularly informative concerning the projectile structures. For the carbon fragments, energy straggling and multiple scattering in the target blur out the structure information in the energy and angle spectra. However, the width of the peak observed in these carbon-ion

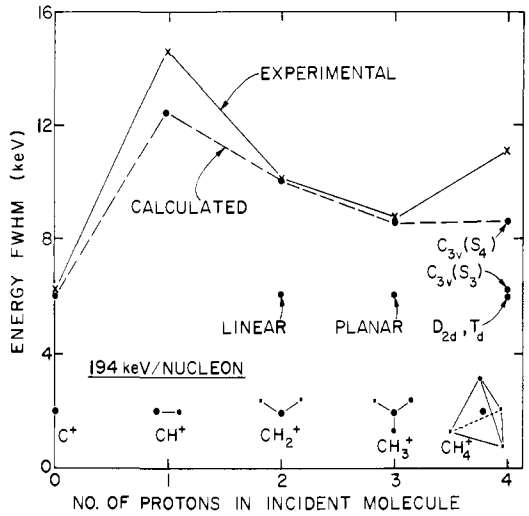

Figure 17. Comparison of energy widths of C^{4+} spectra for $CH_n^+ \rightarrow C^{4+}$. The calculations are based on a carbon ion effective charge of 3.5 and neglect wake forces.[37]

spectra is sensitive to any asymmetry in the distribution of the protons that surround the carbon atom in the projectile.

Figure 17 shows the measured energy widths (fwhm) of outgoing ($\theta = 0$) C^{4+} ions that emerge after the incident beam strikes a foil target. The value of 6.1 keV for incident C^+ represents the contribution of energy straggling convoluted with both the beam energy spread and the resolving power of the electrostatic analyzer system. The Coulomb explosion of the highly asymmetric CH^+ ions adds a large contribution which increases the measured width to 14.6 keV. For the more symmetric CH_2^+ ions, because of near cancellation of the impulses produced by each proton on the carbon ion, the Coulomb explosion is reduced and thus we measure a width of only 10.1 keV. If CH_2^+ were rigidly linear, the width would be expected to be close to the C^+ straggling value of 6.1 keV (the width would actually be somewhat greater than 6.1 keV because of charge-state fluctuation effects that modify the Coulomb explosion while the ion fragments are within the target foil). A similar effect is seen in the measurement of the carbon width for the dissociation of CH_3^+. Again, the width is increased over the minimum that one would expect for a rigid planar structure; however, it is smaller than either of the CH^+ or CH_2^+ results. The data for CH_4^+ show a dramatic departure from this general trend. The measured width of 11.1 keV is larger than all but the CH^+ measurement. This indicates a highly asymmetric proton distribution around the carbon nucleus and is most likely a consequence of the Jahn–Teller distortion of CH_4^+.

The dashed line in Figure 17 shows the width calculated on the basis of a very crude model in which it is assumed that rigid structures having carbon charges of 3.5 and proton charges of 1.0 Coulomb-explode. No attempt was made to include the effects of molecular vibrations, wakes, multiple scattering, charge-state distributions, etc. These calculations thus serve only as a rough guide to the possible structures of the projectiles and are not to be interpreted as determining the actual structures. The calculation for CH^+ assumes a bond length of 1.13 Å. For CH_2^+ a carbon–proton distance of 1.03 Å is assumed and the H–C–H angle is taken to be 140° (a guess based on the expectation that the bond angle will be close to the value of 131° known[36] for the isoelectronic molecule BH_2). For CH_3^+ the calculation assumes a rigid pyramidal structure with an interproton distance of 1.08 Å and with the carbon ion 0.2 Å off the proton plane. The values calculated for CH_4^+ were based on the four Jahn–Teller distorted structures derived by Dixon.[38] As noted above, taking account of vibrational excitations of the projectiles can affect the implications of these calculations. For example, CH_3^+ is commonly thought to be planar[36] and the

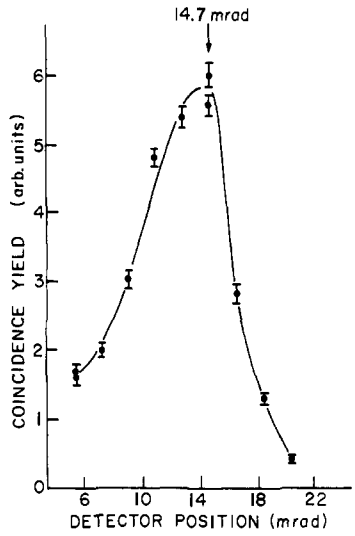

Figure 18. Coincidence counting rate for protons from 3.6-MeV OH_2^+ dissociating in an 80-Å-thick carbon foil.[23] The rate is plotted as a function of the angle between the electrostatic analyzer (set on the low-energy, $\theta = 0$ proton group) and one of the movable surface-barrier detectors (Figure 7).

results shown in Figure 17 are consistent with a planar structure in which a low-frequency out-of-plane oscillation of the carbon ion exists with an amplitude of ~0.2 Å.

Coincidence Measurements

CH_2^+, NH_2^+ and OH_2^+. Preliminary coincidence measurements have been performed for these dihydride ions.[23] Of the three, only OH_2^+ has previously had its structure determined experimentally. From optical measurements Lew and Heiber[39] found the O–H bond length to be 0.999 Å and the H–O–H bond angle to be 110.5°.

Figure 18 shows a spatial scan of the proton–proton double coincidence rate for the foil-induced dissociation of 3.6-MeV OH_2^+ ions. Note that a given combination of post-deflector and electrostatic analyzer (ESA) voltage settings amounts to choosing for study a limited subset of the incoming projectile orientations. For the data shown ion Figure 18, only those OH_2^+ ions in which one proton is trailing are selected. The angular radius of the proton ring pattern is 16.2 mrad. Thus the bond angle is close to $\beta = 180° - \sin^{-1}(14.7/16.2) = 115°$. Approximate corrections for the displaced cm and for the oxygen recoil result in values of 110 ± 2° and 1.0 ± 0.04 Å for the bond angle and bond length, respectively. These values agree with those from the optical measurements.[39] Measurements with other orientations chosen in the ESA give similar results. A more detailed analysis, properly taking into account wake effects and multiple scattering, should result in a significant improvement in the level of accuracy.

Figure 19 shows a comparison of the results for foil-induced dissociation of 3.6-MeV CH_2^+, NH_2^+, and OH_2^+. For these data, the deflections are chosen so that the ESA detects only those protons with the maximum transverse momentum. The double coincidence rate for OH_2^+ peaks a little past the center of the proton cone—again consistent with a bond angle of 110°. However, for the other two projectiles, the peak occurs at the extreme angle of the proton cone—opposite the ESA. This would be consistent with a linear structure, but again vibrational effects may be playing a large role in these projectiles.

We have recently begun triple coincidence measurements, e.g., on the pair of protons and the N^{3+} fragments arising from the dissociation of 3.6-MeV NH_2^+ ions in a dilute Ar gas jet (Figure 20). Although the triple coincidence counting rates are low, the data are very clean and the analysis is simplified as compared with the results obtained with foil targets. In Figure

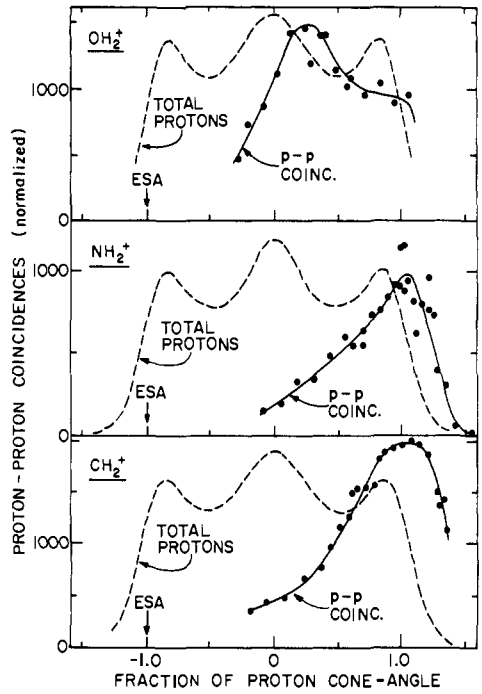

Figure 19. The proton–proton coincidence counting rates for 3.6-MeV beams of CH_2^+, NH_2^+, and OH_2^+ dissociating in carbon foils of thicknesses 98, 66, and 89 Å, respectively.[23] The rates are plotted as functions of the fraction of the proton cone angle (16.25, 14.28, and 13.2 mrad for CH_2^+, NH_2^+, and OH_2^+, respectively) lying between the electrostatic analyzer (set on the protons having the maximum transverse momentum) and one of the movable surface barrier detectors (Figure 7). Also shown are the total (energy-summed) proton-singles rates in the movable detector.

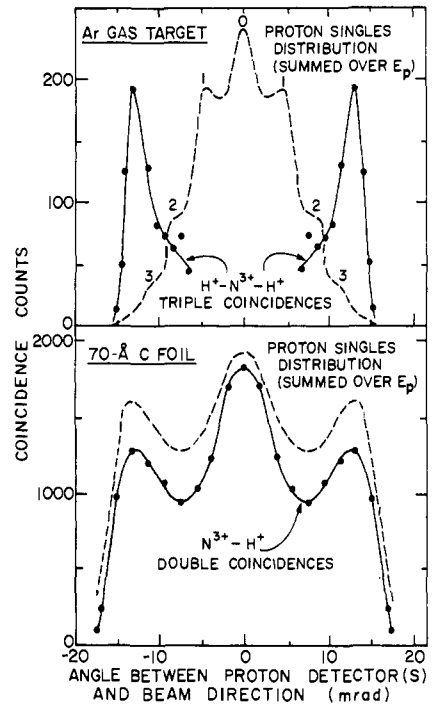

Figure 20. (Top) H^+–N^{3+}–H^+ triple coincidence counting rate for 3.6-MeV NH_2^+ ions dissociating in an Ar gas-jet target. N^{3+} ions are detected at 0 °C in the electrostatic analyzer. Protons are detected in the two movable detectors. The coincidence rate is plotted as a function of the angle between the (symmetrically placed) proton detectors and the beam direction. (Bottom) Same, but double coincidences (N^{3+}–H^+) obtained with a 70-Å carbon foil target. In both figures, the total (energy-summed) proton-singles rates in the movable detectors are shown as dashed curves. In the top figure, the numbers (0, 1, 2, 3) on the dashed curve refer to the corresponding nitrogen ion charge state.[23]

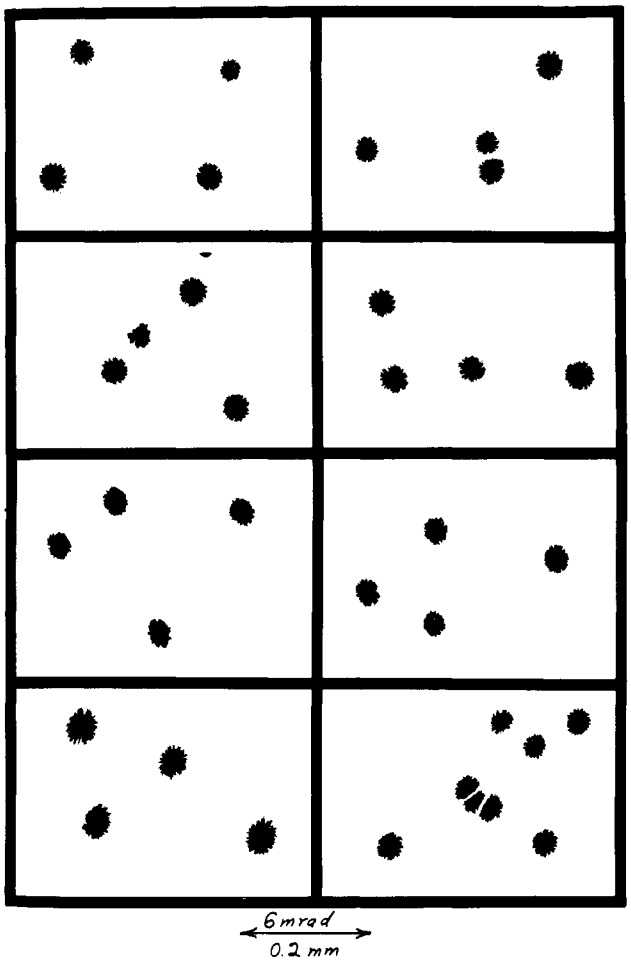

Figure 21. Etched polycarbonate sheet after exposure to fragments from 3.5-MeV C_4^- ions dissociated in a thin carbon foil.[29]

20 the detailed time-of-flight information for each point in the angular scan has not yet been taken into account in the data analysis.

To summarize, we have commenced high-resolution coincidence measurements on the fragments from foil- and gas-induced dissociation of fast polyatomic molecular ions. For OH_2^+, we are able to reproduce the bond angle and bond length found in optical experiments. The precision of the method can now be expected to improve considerably as more refined data-analysis procedures are developed.

Measurements Using Imaging Techniques

At the Weizmann Institute, a photographic technique was developed[31] to study H_3^+. With this technique, all of the fragments from individual projectiles were captured and rendered visible in a photographic emulsion. A similar method has recently been applied by a group at Brookhaven[29] to study the foil-induced dissociation of C_n^- beams. This group uses a polycarbonate plastic sheet as detector. Figure 21 shows such a sheet after exposure to fragments from foil-dissociated C_4^- projectiles. Inferring structure information from data such as these is difficult (except perhaps to observe that C_4^- is not linear). A higher data rate would be very desirable because a statistical analysis of the fragment patterns would then become feasible. Promising steps in this direction are now being taken both at Brookhaven and at Weizmann Institute where electronic imaging techniques are being developed. At Brookhaven[29] a fluorescent screen used in conjunction with an image intensifier is being tested. Workers at the Weizmann Institute[30] have demonstrated that a charge-coupled semiconductor device is capable of acting as a high-resolution two-dimensional detector of charged particles. The energy resolution in each element is expected to be adequate for purposes of distinguishing masses. It is expected that this device will permit the rapid acquisition (~50 images) and storage of two-dimensional projections of individual Coulomb-exploded molecular ions. The digital coordinates of the fragments in each image together with rough measures of their energies will be stored and processed by a computer.

These imaging techniques and the Argonne technique are complementary approaches to the structure problem. The one approach will produce a high rate of coincidences between all fragments for all incident projectile orientations, but little detailed information on energies, charge states, flight times, etc. The other approach selects individual charge states and projectile orientations with very precise information on parameters such as energies, flight times, direction, etc. but with low coincidence counting rates.

Conclusion

We have described the main features of the Coulomb explosion of fast-moving molecular ion projectiles and the manner in which Coulomb-explosion techniques may be applied to the problem (difficult to attack by more conventional means) of determining the stereochemical structures of molecular ions. Examples have been given of early experiments designed to elicit structure information. The techniques are still in their infancy, and it is to be expected that as both the technology and the analysis are refined, the method will make valuable contributions to the determination of molecular ion structures.

Acknowledgments. The research described above has been made possible through the dedicated efforts of an energetic set of collaborators whose names are indicated in the individual references given in this article. The work at Argonne was conducted under the auspices of the Division of Basic Energy Sciences of the U.S. Department of Energy.

References

(1) R. G. Cooks, Ed., "Collision Spectroscopy", Plenum Press, New York, 1978.
(2) E. P. Kanter, P. J. Cooney, D. S. Gemmell, K.-O. Groeneveld, W. J. Pietsch, A. J. Ratkowski, Z. Vager, and B. J. Zabransky, *Phys. Rev. A*, **20**, 834 (1979).
(3) N. Bohr, *K. Dan. Vidensk, Selsk. Mat.-Fys. Medd.*, **18**, 1 (1948).
(4) W. Kolos and J. M. Peek, *Chem. Phys.*, **12**, 381 (1976).
(5) D. S. Gemmell, *Rev. Mod. Phys.*, **46**, 129 (1974).
(6) D. S. Gemmell, J. Remillieux, J.-C. Poizat, M. J. Gaillard, R. E. Holland, and Z. Vager, *Phys. Rev. Lett.*, **34**, 1420 (1975); *Nucl. Instrum. Methods*, **132**, 61 (1976).
(7) J. Neufeld and R. H. Ritchie, *Phys. Rev.*, **98**, 1632 (1955); J. Neufeld and R. H. Ritchie, *Ibid.*, **99**, 1125 (1955).
(8) M. H. Day, *Phys. Rev. B*, **12**, 514 (1975).
(9) Z. Vager and D. S. Gemmell, *Phys. Rev. Lett.*, **37**, 1352 (1976).
(10) R. H. Ritchie, W. Brandt, and P. M. Echenique, *Phys. Rev. B*, **14**, 4804 (1976).
(11) M. Kitagawa and Y. H. Ohtsuki, *Phys. Rev. B*, **16**, 5321 (1977).
(12) Proceedings of the Workshop on Physics with Fast Molecular-Ion Beams, Argonne National Laboratory, Argonne, ILL, Aug 20–21, 1979, D. S. Gemmell, Ed., Physics Division Informal Report ANL/PHY-79-3 (Aug 1979).
(13) A. Breskin, A. Faibis, G. Goldring, M. Hass, R. Kalm, Z. Vager, and N. Zwang, *Phys. Rev. Lett.*, **42**, 369 (1979).
(14) P. M. Echenique, R. H. Ritchie, and W. Brandt, *Phys. Rev. B*, **20**, 2567 (1979).
(15) A. Breskin, A. Faibis, G. Goldring, M. Hass, R. Kalm, I. Plesser, Z. Vager, and N. Zwang, p 1 of ref 12.
(16) A. Breskin, A. Faibis, G. Goldring, M. Hass, R. Kalm, I. Plesser, Z. Vager, and N. Zwang, *Nucl. Instrum. Methods*, **170**, 93 (1980); **170**, 99 (1980).
(17) See, for example, L. C. Northcliffe and R. F. Schilling, *Nucl. Data Tables*, **A7**, 233 (1970).
(18) The Argonne apparatus has evolved over several years. Major contributions to its development have been made by P. J. Cooney, D. S. Gemmell, E. P. Kanter, W. J. Pietsch, I. Plesser, A. J. Ratkowski, Z. Vager, and B. J. Zabransky.
(19) Z. Vager, D. S. Gemmell, and B. J. Zabransky, *Phys. Rev. A*, **14**, 638 (1976).
(20) D. S. Gemmell, P. J. Cooney, W. J. Pietsch, A. J. Ratkowski, Z. Vager, B. J. Zabransky, A. Faibis, G. Goldring, and I. Levine, Proceedings of the 7th International Conference on Atomic Collisions in Solids, Moscow, Sept 19–23, 1977, to be published.

(21) D. S. Gemmell, "Radiation Research" (Proceedings of the Sixth International Congress of Radiation Research, Tokyo, Japan, May 13-19 1979), S. Okada, M. Imamura, T. Terashima, and H. Yamaguchi, Eds., University of Tokyo, 1979, pp 132-144.
(22) D. S. Gemmell, *Nucl. Instrum. Methods*, **170**, 41 (1980).
(23) D. S. Gemmell, P. J. Cooney, and E. P. Kanter, *Nucl. Instrum. Methods*, **170**, 81 (1980).
(24) D. S. Gemmell, I. Plesser, and B. J. Zabransky, private communication.
(25) J. Golovchenko and E. Laegsgaard, *Phys. Rev. A*, **9**, 1215 (1974).
(26) R. Laubert and F. K. Chen, *Phys. Rev. Lett.*, **40**, 174 (1978).
(27) M. J. Gaillard, J.-C Poizat, and J. Remillieux, *Phys. Rev. Lett.*, **41**, 159 (1978).
(28) D. S. Gemmell, E. P. Kanter, I. Plesser, and Z. Vager, private communication.
(29) G. Goldring, Y. Eisen, P. Thieberger, and H. Wegner, p 27 of ref 12.
(30) M. Algranati, A. Faibis, R. Kalm, and Z. Vager, private communication.
(31) M. J. Gaillard, D. S. Gemmell, G. Goldring, I. Levine, W. J. Pietsch, J.-C. Poizat, A. J. Ratkowski, J. Remillieux, Z. Vager, and B. J. Zabransky, *Phys. Rev. A*, **17**, 1797 (1978).
(32) G. D. Carney, *Mol. Phys.*, **39**, 923 (1980).
(33) D. L. Smith and J. H. Futrell, *J. Phys. B*, **8**, 803 (1975).
(34) G. D. Carney and R. N. Porter, *J. Chem. Phys.*, **65**, 3547 (1976).
(35) D. S. Gemmell, E. P. Kanter, and W. J. Pietsch, *Chem. Phys. Lett.*, **55**, 331 (1978).
(36) G. Herzberg, "Electronic Spectra of Polyatomic Molecules", Van Nostrand, Princeton, NJ, 1950.
(37) D. S. Gemmell, E. P. Kanter, and W. J. Pietsch, *J. Chem. Phys.*, **72**, 1402 (1980).
(38) R. N. Dixon, *Mol. Phys.*, **20**, 113 (1971).
(39) H. Lew and I. Heiber, *J. Chem. Phys.*, **58**, 1246 (1973); H. Lew, *Can. J. Phys.*, **54**, 2028 (1976).